Average Seasonal Variation of the Atlantic Equatorial Currents from Historical Ship Drifts[1]

P. L. RICHARDSON AND T. K. MCKEE

Woods Hole Oceanographic Institution, Woods Hole, MA 02543

(Manuscript received 28 December 1983, in final form 27 April 1984)

ABSTRACT

Surface currents in the tropical Atlantic were studied using historical ship-drift data. These are the only available data capable of resolving the long-term seasonal fluctuations of currents over a broad geographical region. The North Equatorial Countercurrent was found to extend as a continuous eastward-flowing current across the Atlantic in the band 5–8°N from July to December. The maximum average eastward velocity was ~30 cm s^{-1} during July–September. East of 20°W the countercurrent continued throughout the year. West of 20°W and from January to June the countercurrent disappeared and westward currents were observed. Average westward velocity reached 20 cm s^{-1} in April and May, centered near 40°W. The annual cycle in surface velocity (20 cm s^{-1} amplitude) agrees closely with that of geostrophic velocity inferred from variations in thermocline depth across the countercurrent, as determined recently by Garzoli and Katz. The South Equatorial Current contains two swift westward current jets, centered near 2°N and 4°S, separated by a minimum near 1°S. The northern jet has a large (14 cm s^{-1} amplitude) semiannual variation. The fastest velocity, 61 cm s^{-1}, occurs in June corresponding to a rapid increase in eastward velocity in the Countercurrent. Large values of eddy kinetic energy coincide with the locations and times of strong shear between the Countercurrent and the northern jet of the South Equatorial Current.

1. Introduction

The Atlantic North Equatorial Countercurrent (NECC) responds strongly to seasonal atmospheric forcing. During summer and fall each year, the NECC flows eastward between ~3 and 10°N with speeds up to 50 cm s^{-1}; during winter and spring this current disappears and velocities are westward. This is a very different situation from the Pacific NECC, which weakens in winter but does not disappear (Wyrtki *et al.* 1981). Though the Atlantic NECC is important to the understanding of the general circulation and the forced response of the tropical Atlantic, this current has not been well described. This is partially because of the lack of long-term current measurements. Aside from ship-drift velocities, the only direct measurements of near surface currents in the NECC are a few drifting buoys (J. D. Cochrane, personal communication, 1983; Molinari, 1983) and some current-meter measurements made during GATE (Bubnov and Egorikhin, 1979; Halpern, 1980) which are too short to show seasonal variations.

Thus, the primary sources of information on surface currents are ship-drift vectors. [Over 200 years ago Captain James Cook made some of the first ship-drift measurements in the tropical Atlantic and described the primary surface current system (Beaglehole, 1955–67).] Although some seasonal vector maps exist (Schumacher, 1940), these data have not yet been used very quantitatively. One objective of the present work was to use ship-drift data to examine the seasonal variation of surface currents in the tropical Atlantic more quantitatively than has been done before. A second objective was to prepare maps of currents to help plan the deployment locations in the NECC of surface drifters and a current-meter mooring. These were deployed as part of SEQUAL (Seasonal Equatorial Atlantic Experiment; see Anon, 1983). A third objective was to obtain a characterization of the average seasonal variation of currents with which to interpret the year-and-a-half measurements to be made during SEQUAL. A fourth objective was to assemble a historical data set with which to compare model predictions.

One rather surprising result was that the ship-drift data gave a clear and consistent portrayal of seasonal variations of surface currents. This is surprising because of the many problems and errors in measuring current velocity from the drift of a ship at sea. When sufficiently large numbers of individual observations are combined in a calculation of mean velocity, however, the random errors are reduced to a level well below the dominant seasonal variations. Some variations observed here have also been observed in historical hydrographic data (Garzoli and Katz, 1983; Merle, 1983).

[1] Woods Hole Oceanographic Institution Contribution No. 5583.

2. Data and methods

The ship-drift velocity data were obtained from the U.S. Naval Oceanographic Office. They consist of approximately 438 000 individual observations within the region bounded by 20°S–20°N, 10°E–70°W, and the coasts of Africa and South America. Most observations were made from United States ships; about a third were obtained from the Netherlands.

Each ship-drift measurement of surface current velocity consists of the vector difference between the velocity of a ship determined from two position fixes and the average estimated velocity of the ship through the water during the same time interval, usually 12–24 hours. The vector difference is considered to be due to a surface current. Each measurement is an average 1) over the depth of the ship's hull and 2) along the ship's path between fixes, usually a few hundred kilometers. Thus only larger-scale features, greater than a few hundred kilometers, can be resolved using this technique.

Many possible random and systematic errors can occur during ship-drift measurements, and it is difficult with the available information to evaluate the errors very accurately. Windage on the ships could lead to a systematic error in surface velocity. A single velocity measurement is estimated to have a random error of $\sim$20 cm s^{-1}. This is based on a combination of the estimated errors of both position fixes and dead reckoning. Values used as typical random errors of position, direction and speed are $\pm$2 km, $\pm$1° and $\pm$0.3 knots. The size of the standard error of the mean velocity can be reduced considerably by combining large numbers of observations. With 100 observations, the standard error of mean velocity decreases from 20 to 2 cm s^{-1}. The number of observations used to calculate mean velocity was often greater than 100, even in monthly subsets of the data.

The observations are not homogeneously distributed in space and time. Most ships followed standard sailing routes along which the data density is as high as 100–500 observations per 1° square (Fig. 1). Fortunately, many routes follow coasts and many others cut across the central equatorial region, covering both the boundaries and the internal regions. Between these lines, the data density is reduced to 10–50 observations per 1° square. Within the NECC, the region centered near 35°W contains a low data density. Some low-data-density regions could be contaminated, as a result of position mistakes, by velocity values really measured in neighboring high-data-density regions.

Most of the observations that have a known year were made between 1920 and 1940 (Fig. 2a). At the end of 1941 the number of observations dropped precipitously, from about 11 000 to 500 per year. It never again rose to pre-World War II levels. Some of the 34% of the observations without a known year, however, could have come after 1941.

The data are very evenly distributed seasonally (Fig. 2b). The average number of observations each month is $\sim$35 000. December has the fewest with 27 000, and August the most with 41 000.

In order to calculate and map mean velocity values, individual velocity values were grouped into various

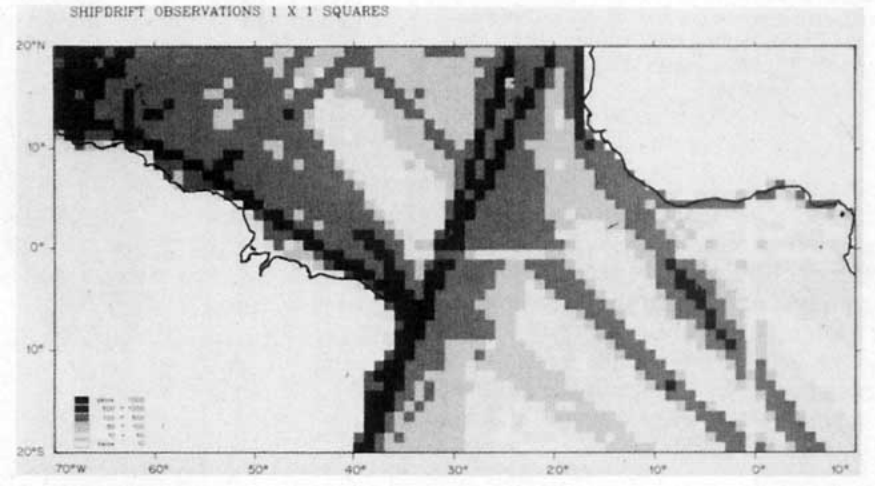

FIG. 1. Distribution in 1° squares of the 438 000 ship-drift velocity observations. The main ship routes are seen as dark bands, where the data density is over 100 observations per 1° square. The darker squares that lie along the route from 20°S, 40°W to 20°N, 20–25°W have a density from 500 to 1000 observations per square. The two light bands that lie between 0–1°S and 0–1°W occur because 1) position values were often rounded to the nearest whole degree and 2) values of 0° latitude were assumed to lie in the band 0–1°N and those at 0° longitude in the band 0–1°E.

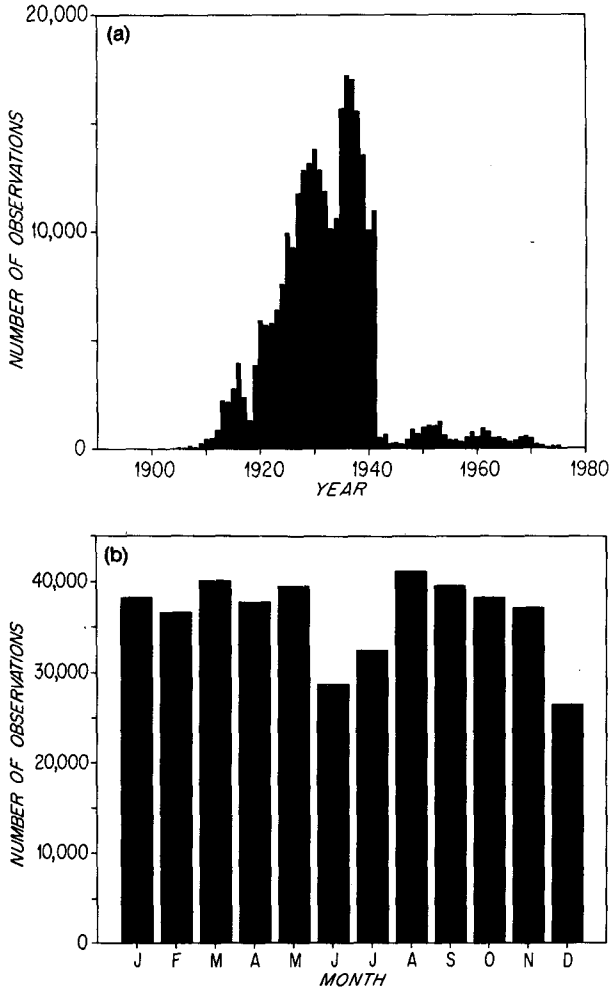

FIG. 2. Distribution of velocity observations as a function of (a) year of the 289 000 ship-drift observations that have a known year. An additional 700 observations before 1900 are not shown. No year was available for 149 000 observations (34% of the total). (b) Velocity observations for each month.

sized space–time boxes. First, 12 monthly maps were made from 1° latitude × 3° longitude boxes. Some of the monthly maps were similar. These were grouped together to produce characteristic velocity fields showing the maximum and minimum velocity in the NECC in August–October and February–April. Some features, such as the NECC and South Equatorial Current, were investigated by computing monthly velocities in zonal bands along these currents and in north–south sections across them.

3. Results

a. Equatorial currents

The annual mean velocity distribution near the central tropical Atlantic is shown in Fig. 3, and two maps of the surface currents are shown in Fig. 4, one for the time when the NECC flows strongly eastward and one when the NECC has disappeared. Three major currents are clearly identified. North of 10°N is the westward-flowing North Equatorial Current (NEC) which has an average speed of 10 cm s^{-1}. Between ~5 and 10°N is the eastward-flowing NECC, with a maximum (annual average) speed of 8 cm s^{-1}. South of 5°N is the westward-flowing South Equatorial Current (SEC) which has two maxima with average speeds of ~35 cm s^{-1}, located at 2°N and 4°S. The NECC is a region of weak meridional velocity and strong meridional convergence. Water enters the NECC from the SEC along its entire length and from the NEC along its eastern portion. The equator has zero meridional velocity and strong divergence.

During February–April the current is westward everywhere except in the eastern NECC and the Guinea Current. Fastest westward speeds are in the SEC which is centered near the equator in the east (0–10°W). In the central Atlantic, the SEC divides into two westward flowing jets centered at 2 and 4°N. The southern jet impinges on and runs along the north coast of Brazil as the North Brazil Current, part of which continues into the Caribbean. [The northwestward current that runs along the coasts of Brazil, French Guiana, Surinam, Guyana and Venezuela, and into the Caribbean will be referred to here

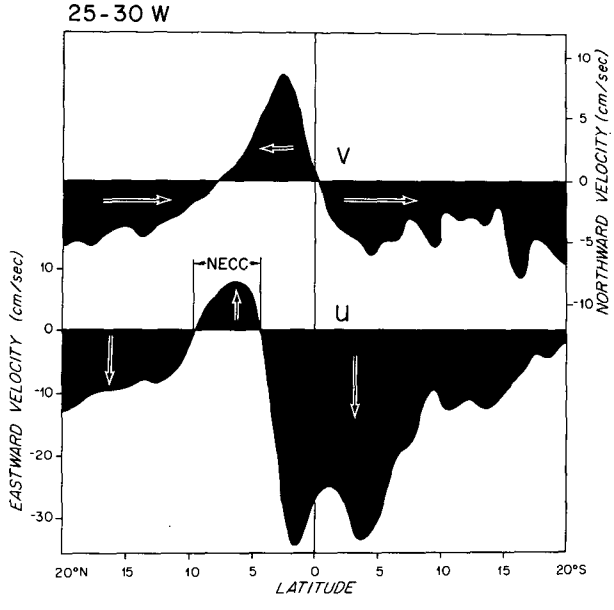

FIG. 3. North–south section of annual average velocity components calculated for 1° latitude × 5° longitude boxes in the central Atlantic at 25–30°W. The mean zonal currents consist of the westward flowing North Equatorial Current located north of 10°N, the eastward flowing North Equatorial Countercurrent (NECC) between ~5 and 10°N, and the westward flowing South Equatorial Current with maxima near 2°N and 4°S. The NECC is a region of meridional convergence and the equator a region of meridional divergence. The small scale variations in the velocity components south of 5°S are due to the low data density there (see Fig. 1).

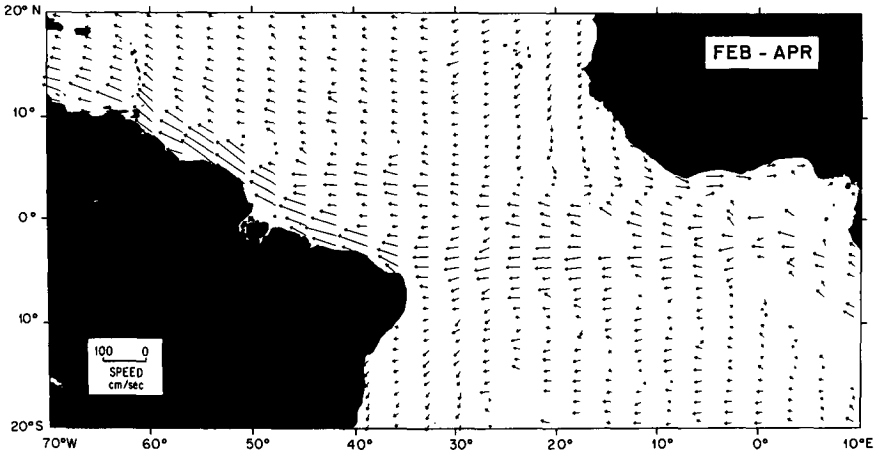

FIG. 4a. Map of velocity vectors calculated with data grouped into 1° latitude × 3° longitude boxes for the 3-month period February–April, when the NECC has disappeared west of 20°W. Vectors in boxes containing fewer than ten observations were omitted. Speed is given by the length of the tail of each vector.

as the North Brazil Current. Between the tip of Brazil and the mouth of the Amazon at about 50°W this current has been called the North Brazil Coastal Current and northwest of this region the Guiana Current (Metcalf and Stalcup, 1967).] The northern jet of the SEC merges with this current near 4°N, 50°W.

During August–October, the North Brazil Current retroflects between 45 and 53°W, forming the western extremity of the NECC. From there the NECC flows eastward across the Atlantic in the band 5–8°N, merges with the Guinea Current near the coast of Africa, and flows into the Gulf of Guinea where ship-drift velocities are too sparse to resolve the velocity field. The water might be recirculated in the SEC, which flows westward near the equator there.

b. Monthly variations

Monthly variations in the equatorial currents can be seen in three north–south velocity profiles (Figs. 5a–c) and in velocity time series (Fig. 6). The first profile is near the center of the Atlantic between 25 and 30°W. The second is in the west between 35 and 45°W and extends to the north coast of South America. The third is in the east between 10 and 20°W, and adjacent to the coast of Africa (north of 5°N).

In the central Atlantic (Fig. 5a) the NECC begins quickly in June, centered near 6°N. During August–October it flows steadily (in a monthly time-average sense) between 4 and 11°N, with a maximum speed of about 34 cm s^{-1}. During November and December

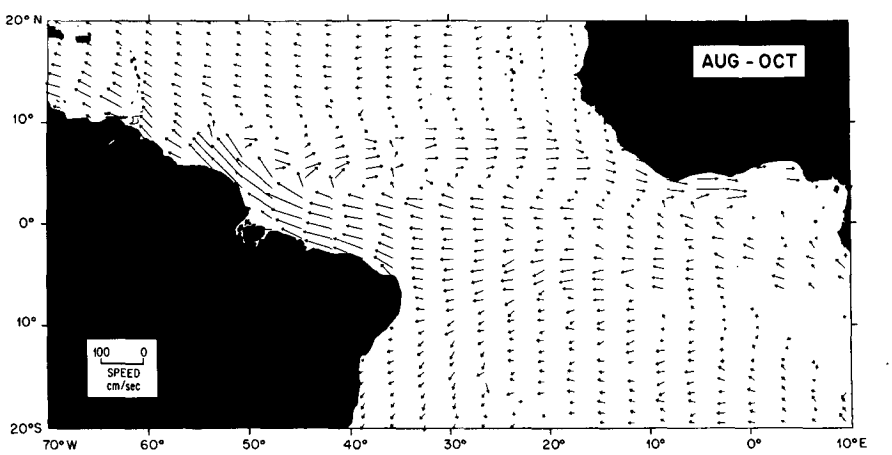

FIG. 4b. Velocity vectors for the 3-month period August–October when the NECC is flowing strongly eastward. Eastward vectors form a continuous band across the Atlantic, except near 35°W where the vectors are noisy because of the low data density there.

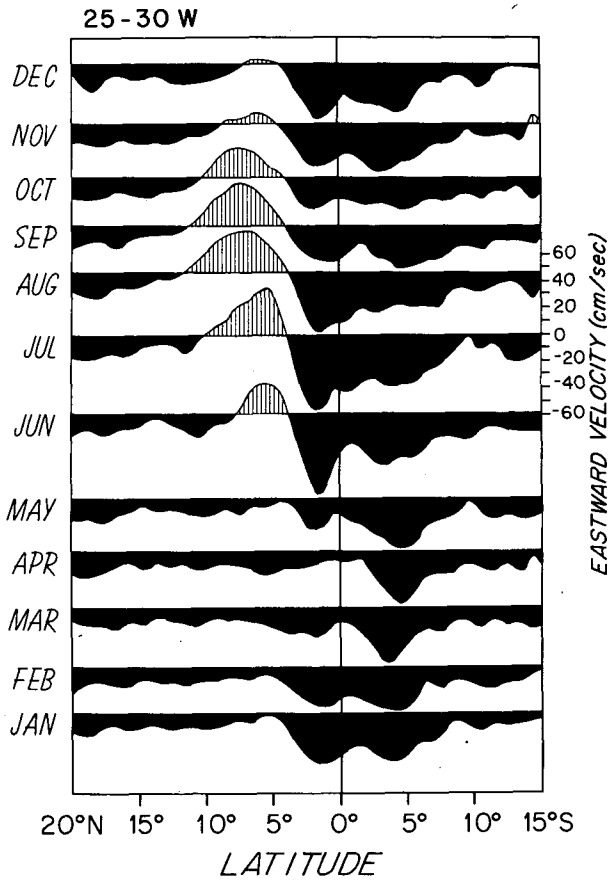

FIG. 5a. Monthly north–south profiles of zonal currents in the central Atlantic at 25–30°W. The NECC begins suddenly in June accompanied by an intensification of a westward jet located near 2°N. The NECC continues through December with peak speeds of 34 cm s^{-1} in July–September.

it gradually decays and by January it disappears. The dominant period is annual with an amplitude of 20 cm s^{-1} (Fig. 6, Table 1).

During the sudden beginning in June of the NECC, the northern jet in the SEC, located near 2°N, has a corresponding sudden increase of speed from 24 cm s^{-1} in May to 61 cm s^{-1} in June. This results in a strong shear between the NECC and the SEC of ~90 cm s^{-1} (over 4° latitude) in July. The velocity in the northern jet of the SEC has a dominant semiannual period (amplitude 14 cm s^{-1}) with peaks in June and December (Fig. 6, Table 1). The southern jet of the SEC, located near 4°S, has smaller monthly fluctuations that appear to be dominated by an annual period. During September–February the two jets are nearly equal in velocity; during June–August the northern jet is faster and during March–May the southern jet is faster.

The monthly variations of zonal currents in the central Atlantic are mainly confined to the region located between 10°S and 15°N. Poleward of this latitude band the westward velocity is ~10 cm s^{-1} and quite steady. The small-scale geographical variation in profiles outside this band is probably an indication of the inaccuracy of ship-drift velocities. The southern region has slightly larger variations due to a lower data density.

No South Equatorial Countercurrent is observed. A patch of consistently eastward velocity of ~5 cm s^{-1} does occur in November and December, centered near 15–20°S, 25–35°W (based on 1 × 3° monthly values). Because this eastward velocity is accompanied by a large southward component of ~12 cm s^{-1}, the flow is primarily meridional. The patch does not extend zonally across the Atlantic, as does the NECC.

In the western velocity profile (Fig. 5b) the NECC begins earlier and continues later. It is first seen in

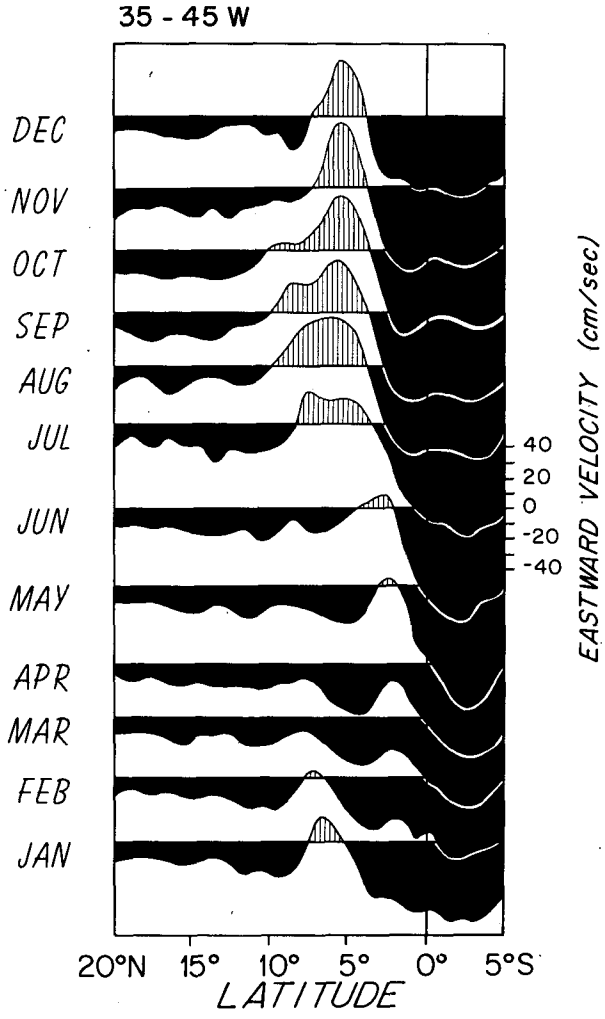

FIG. 5b. Monthly north–south profiles of zonal velocity near the coast of Brazil at 35–45°W. Velocity values were computed from data grouped into 1° latitude × 10° longitude boxes. The NECC begins in May near 2–3°N, shifting northward and stabilizing near 3–10°N from July through December. In January and February it weakens and by March it disappears.

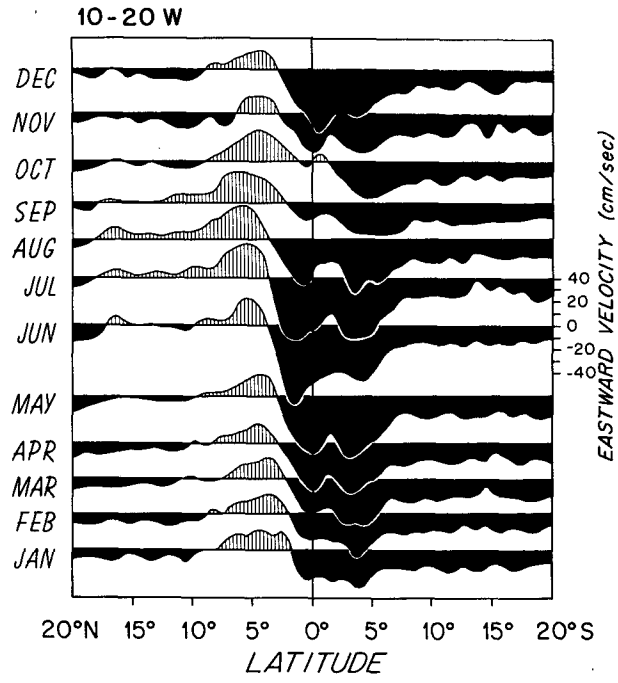

FIG. 5c. Monthly north–south profiles of zonal velocity near the coast of Africa at 10–20°W. The NECC and its continuation into the Guinea Current occurs throughout the year. Maximum eastward velocities occur in July–October between 3 and 10°N.

May near 2–3°N. From May to July it migrates northward, and during August–October it assumes a quasi-steady position between 3 and 10°N, with a peak speed of 36 cm s^{-1}. It narrows in November but continues as an eastward current through February. In March and April no eastward velocity is seen, but two minima in the westward velocity (at 2 and 8°N) occur at the latitudes where the eastward velocity will appear in May and where it disappeared in February. Thus, there is a suggestion that an incipient NECC from one year coexists briefly with the remnant NECC from the previous year.

In the western area the double-jet structure of the SEC is weakly defined and only present from August to November. Over most of the year the jets merge, forming a single maximum near 2–3°S. The maximum westward speed of this jet is 80 cm s^{-1} and this occurs in May. In March–May, the incipient NECC located near 2°N divides the westward flow, causing the appearance of a westward jet with speeds of 30 cm s^{-1}, located near 4°N.

In the eastern velocity profile (Fig. 5c), the NECC occurs throughout the year, centered between 2 and 8°N. The southern boundary shifts northward to 4°N in June–August and southward to 2°N in January and in October. The northern boundary shifts northward, reaching 17–18°N in July–September. Maximum velocity is ~28 cm s^{-1} in July and August and is centered near 5°N.

The northern jet of the SEC fluctuates strongly with a semiannual period in this eastern area. In June a maximum speed of 66 cm s^{-1} is observed near 2°N. Minima occur in October and February. During most of the year, the northern jet lies close to the equator. In some months (December–February), it merges with the southern jet to form a single broad jet. The southern jet has a maximum velocity of 50 cm s^{-1} near 4°S during May–July. South of 10°S the velocity is very constant in time, with speeds of ~15 cm s^{-1}.

The minimum in velocity centered between the SEC jets near 1°S is probably an indication of the eastward flowing equatorial undercurrent. Models suggest that southerly winds force an upwelling south of the equator and a southward shift of the undercurrent (Cane, 1979; Philander and Pacanowski, 1981). The upwelling and also vertical momentum transport due to mixing retard the surface current just south of the equator causing a minimum in westward velocity there.

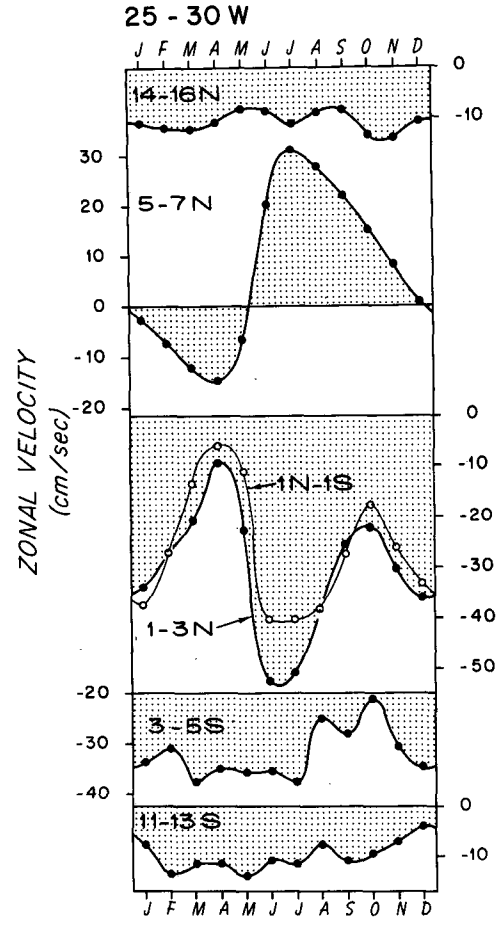

FIG. 6. Time series of monthly zonal velocity in the central Atlantic at 25–30°W. The variation in NECC velocity is primarily annual; that of the northern jet of the SEC and at the equator is semiannual.

TABLE 1. Summary of the annual and semiannual harmonics of zonal velocity in the central Atlantic at 25–30°W.

Current	Latitude band	$\bar{u}$ (cm s^{-1})	Annual period		Semiannual period	
			Amplitude (cm s^{-1})	Phase (deg)	Amplitude (cm s^{-1})	Phase (deg)
NEC[a]	14–16°N	−10.5	1.6	78	0.6	301
NECC[b]	5–7°N	7.0	20.2	146	7.3	308
SEC[c]	1–3°N	−30.5	7.4	313	14.1	102
SEC	1°S–1°N	−26.2	7.2	350	14.0	117
SEC	3–5°S	−32.1	5.0	190	2.9	73
SEC	11–13°S	−10.0	2.8	222	1.4	251

[a] North Equatorial Current.
[b] North Equatorial Countercurrent.
[c] South Equatorial Current.

c. *North Equatorial Countercurrent*

The limits of the NECC for each month are shown in Figure 7. These were obtained by contouring the areas of eastward velocity plotted in 1° latitude × 3° longitude boxes for each month. The NECC is formed by the westward progression of eastward flow originating near 20°W in March, and by the northward progression of eastward flow originating near 40°W just north of the equator in May. In July the NECC extends as a coherent eastward current across the Atlantic. The limits of this current continue to expand northward and westward, reaching the greatest extent in August–October. From November through January it contracts latitudinally and by January and February it becomes discontinuous and difficult to contour. By March the eastward flow has disappeared west of 20°W.

Figure 7 shows a more continuous NECC than that given by Boisvert (1967), who showed a break near 35°W in October–December. This difference is a result of the low data density in this region, which causes the velocity vectors to be noisy there. We conclude here that there is a gap in the data at 35°W, not a gap in the NECC.

The continuity of the NECC and its seasonal variation is clearly shown on a time–longitude diagram of zonal velocity between 5 and 8°N (Fig. 8a). This band is divided geographically into three different zones. West of 50°W, the North Brazil Current always flows westward, reaching a maximum speed of 62 cm s^{-1} in April. East of 20°W the NECC always flows eastward, reaching a maximum speed of 24 cm s^{-1} in September. Between these two longitudes the NECC changes direction seasonally. From July to January it flows continuously eastward across the Atlantic. Peak velocity is 37–38 cm s^{-1} in July and August. West of 20°W, the NECC disappears each year from February to June and is replaced by westward velocity. The first westward velocity is seen in the region near 30°W; peak westward velocity is 21 cm s^{-1} near 40°W in May.

The velocity contours (Fig. 8a) and distribution of eastward velocity (Fig. 7) suggest the presence of a westward phase propagation with a speed of ~40 cm s^{-1}. This value is characteristic of the decay of the NECC on Fig. 8a. The start-up of the NECC has a faster apparent phase speed (Fig. 8a) because of the merging of the northward migrating patch of eastward flow located near 40°W (Fig. 7).

The meridional flow is always northward in the North Brazil Current with a maximum speed of 48 cm s^{-1} in May, and generally southward in the eastern NECC with maximum speeds of 12 cm s^{-1} in January and February (Fig. 8b). Over most of the

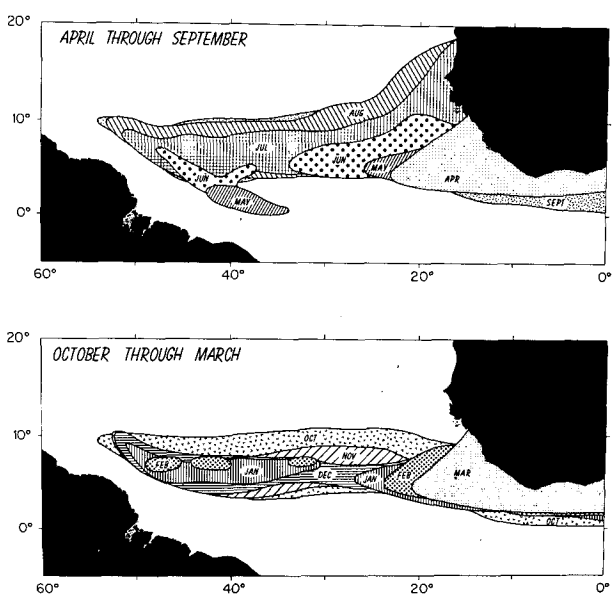

FIG. 7. Monthly limits of the eastward velocity in the NECC. The top panel shows the westward and northward progression of the NECC from April through September. The lower panel shows the relaxation of the NECC from October through March. From July through December the NECC is a continuous eastward current extending across the Atlantic. This figure is similar to one given by Boisvert (1967).

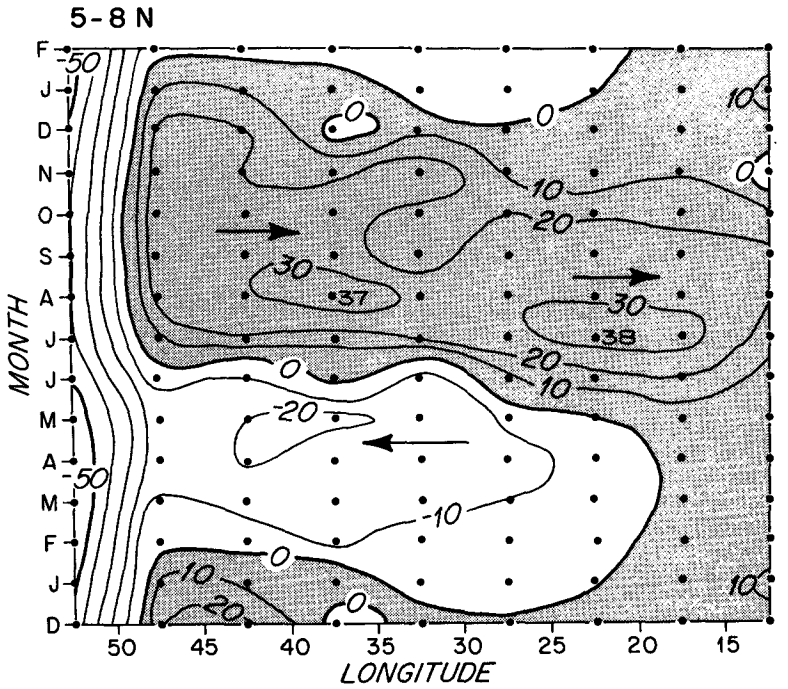

FIG. 8a. Time-longitude plot of eastward velocity (cm s^{-1}) in the NECC. Velocity values were calculated from observations grouped into 3° latitude × 5° longitude boxes lying along the band 5–8°N and extending from 10 to 55°W. Between 20 and 50°W the NECC reverses seasonally. East of 20°W the NECC always flows eastward. West of 50°W the North Brazil Current always flows westward. This figure is similar to one given by Garzoli and Katz (1983).

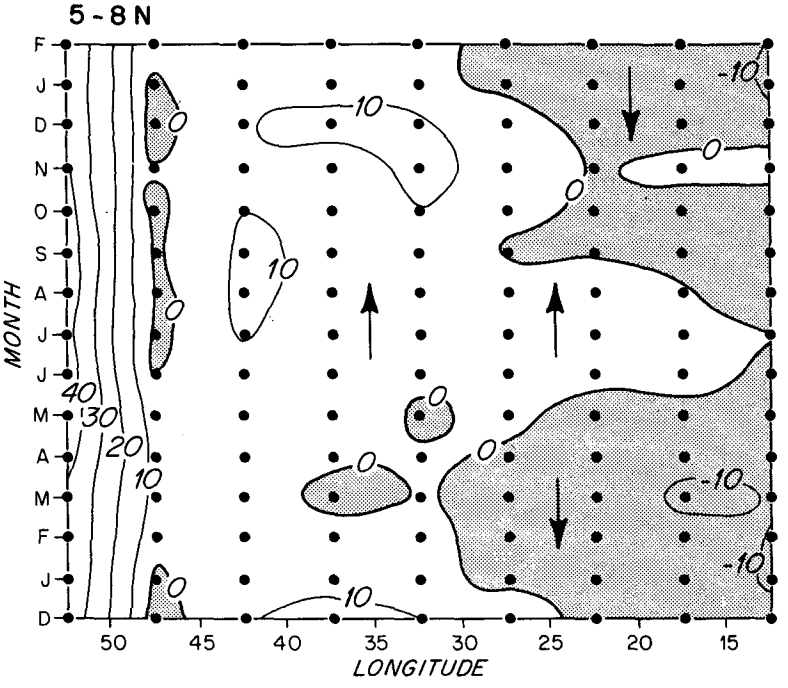

FIG. 8b. As in Fig. 8a but for northward velocity (cm s^{-1}).

NECC the flow is predominantly northward, with maximum speeds reaching 16 cm s^{-1}. East of about 40°W, southward velocities occur seasonally, centered in the time during January–April. Another region of southward velocity occurs between 45 and 50°W from June to January; this is a result of the southward deflection of the NECC near 45°W.

The western extremity of the NECC and this deflection are shown in detail in Fig. 9a. August is chosen because the current vectors have stabilized during this month. The western extremity of the NECC is formed from the North Brazil Current, part of which retroflects near 45–53°W and flows swiftly to the southeast parallel, but counter to the North Brazil Current. This western NECC has velocities up to 60 cm s^{-1} (in September) and a width of about 300 km. Near 5°N, 40–50°W, the southeastward flow encounters the northwestward flowing SEC and North Brazil Current. The two opposite flows converge and turn northeastward and then eastward, forming the main NECC. The northward flow of water from the SEC into the NECC occurs all the way across the Atlantic (Fig. 4b), but it is strongest in the west between 40 and 45°W.

A contrasting velocity field is shown for April (Fig. 9b), when the NECC has disappeared. No consistent eastward flow is observed. During May the retroflection of the North Brazil Current is located near 3°N, 42°W and the eastward flow is observed as far south as the equator near 36°W; during the period May–July the retroflection and the patch of eastward flow migrate northwestward along the coast (Fig. 7).

d. Current along the equator

The seasonal variation of zonal currents along the equator is shown on a time-longitude plot in Fig. 10. Except for three small regions (10–15°W in October,

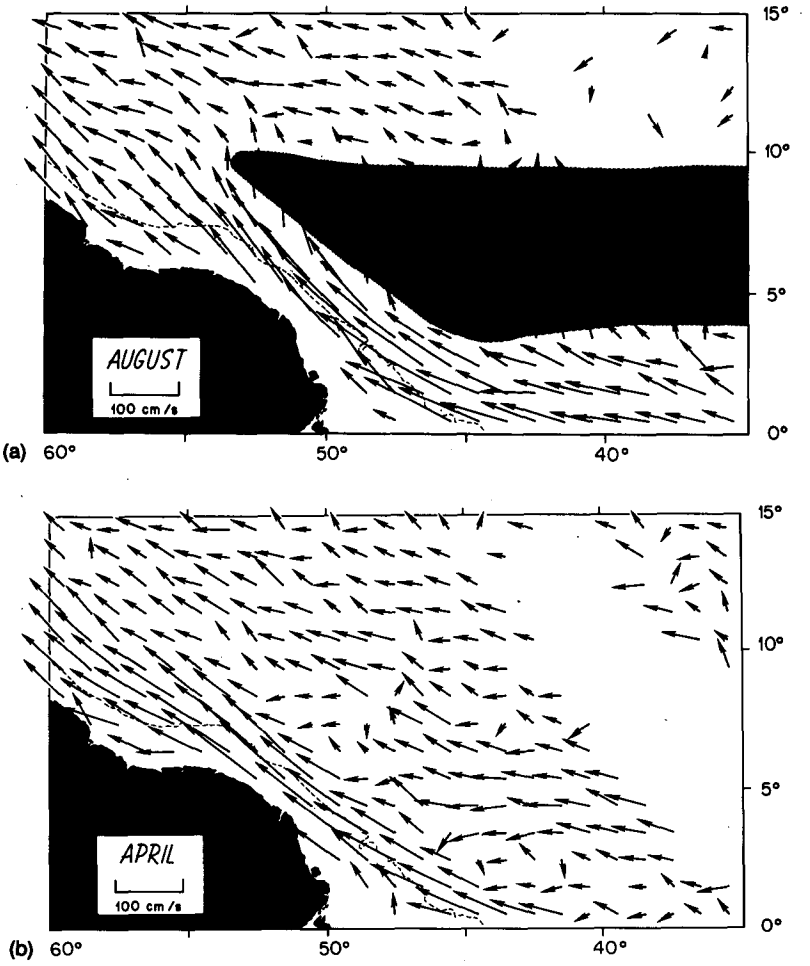

FIG. 9. Map of velocity vectors in the western NECC computed for (a) August and (b) April from data grouped into 1° squares. Speed is given by the length of the tail of each vector. Vectors were omitted in boxes containing fewer than five observations. The region of eastward velocity has been shaded to show the NECC.

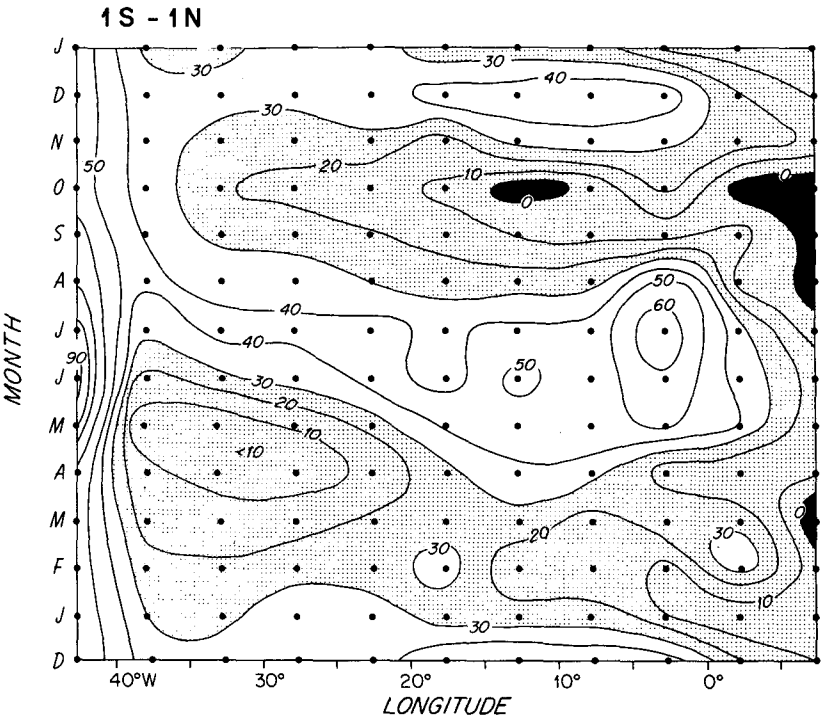

FIG. 10. Time–longitude plot of westward velocity along the equator. Velocity values were computed from data grouped into 2° latitude × 5° longitude boxes in the band 1°S–1°N from 10°E to 45°W. Velocities less than 30 cm s^{-1} are shaded, and eastward velocities are black to emphasize certain features. East of 5°W the data density is very low. The variation of monthly velocity has a dominant semiannual period.

0–10°E in August–October and 5–10°E in May) the velocity is always westward. Maximum velocity (90 cm s^{-1}) occurs in the far west (40–45°W) where the North Brazil Current crosses the equator. The major patterns in Fig. 10 are 1) a strong semiannual fluctuation that occurs east of 40°W and 2) an apparent westward phase shift located geographically from 15 to 40°W and seasonally from February to August. During the first half of the year, the semiannual fluctuation has a minimum velocity occurring first (January–March) in the east (near 0°W) and later (April and May) in the west (30–35°W). This is followed by a maximum in June–August during which the highest westward speeds reach 65 cm s^{-1} in the Gulf of Guinea at 0–5°W. During the second half of the year, the semiannual fluctuation has a minimum (<20 cm s^{-1}) in October and maximum (>30 cm s^{-1}) in December. These extremes extend simultaneously across the Atlantic, although their amplitude varies with longitude, becoming greatest, ~25 cm s^{-1}, near 10°W. It is cautioned that, east of 5°W, data are scarce along the equator (Fig. 1), and velocity values therefore tend to be noisier than west of 5°W. Another minimum in data exists near 15°W.

The timing of the increase of velocity in April–August west of 15°W matches the beginning of the NECC and the concomitant increase in velocity of the northern jet of the SEC. The southern flank of this jet overlies the equator. Thus, the semiannual signal along the equator reflects the variation of this jet.

The variation of zonal velocity along the equator has some similarities to the variation of zonal wind stress along the equator. Both surface velocity and wind stress have a minimum in January–May and a maximum in July–August, and both have the same westward phase propagation (Hastenrath and Lamb, 1977; Picaut, 1983; Weisberg and Tang, 1983). The wind stress has a secondary peak in November which occurs simultaneously all along the equator (west of 0°W). This is similar to the zonal velocity, with the exception that the velocity of this peak occurs in December.

There have been numerous reports of fast eastward velocities (~50 cm s^{-1}) along the equator near 25–35°W (Schumacher, 1940; Neumann, 1960; Voigt, 1961; Stalcup and Parker, 1965; Katz *et al.*, 1981; Katz and Garzoli, 1982; Weisberg and Tang, 1983). The eastward velocity occurs in the spring (March to May) and is associated with the relaxing of the easterly trades at that time. When the wind stress relaxes, the zonal pressure gradient accelerates an

eastward velocity in the surface layer which augments the transport of the undercurrent.

Although eastward velocity was not observed in the monthly average values of ship drift in this area (Fig. 10), a minimum of westward velocity (1 cm s^{-1}) was clearly observed in April–May between 25 and 40°W. Approximately 40% of the observations near this minimum were of eastward velocity. An average of just these eastward velocities is 25 cm s^{-1}. Monthly values calculated on a finer grid (1 × 3° boxes) do resolve an eastward velocity of 7 cm s^{-1} in May centered near 35°W and between 0 and 1°N (Fig. 7). This is associated with a patch of eastward velocity that extends from 0 to 3°N in May and that migrates northward to become the western NECC in June and July. Eastward velocity is not resolved in Fig. 10 because the averaging of velocities in larger boxes (2 × 5°) tends to smooth over smaller-scale temporal and spatial features. Thus, there is no conflict between these results and earlier reports.

e. Eddy kinetic energy

A measure of the time-variability of the surface currents is given by the eddy kinetic energy, which is the average of the variance of velocity about the mean in the east and north directions. Figure 11a shows the geographical distribution of eddy kinetic energy (per unit mass) computed from all data in each 1° square. A slightly different presentation of the same results north of the equator has been given by Wyrtki *et al.* (1976). Figure 11a shows a broad maximum in energy with values greater than 400 cm^2 s^{-2} lying between approximately 10°S and 10°N. Within these limits lie two peaks. The highest values of eddy energy lie along the coast of South America from 3°S to 9°N and in a tongue projecting eastward toward 30°W along 5°N. Values of 1800–1900 cm^2 s^{-2} are observed near 5°N, 45°W. This is the area where the North Brazil Current runs northwestward, turns offshore, and then runs eastward forming the NECC (Fig. 4). The second peak occurs farther east, between 0–4°N and 0–30°W, where values of about 1000 cm^2 s^{-2} are observed. This region lies near the boundary between the NECC and the northern jet of the SEC, an area of strong shear in the zonal currents and also of strong seasonal variability.

The geographical pattern of eddy kinetic energy also fluctuates seasonally. The maxima of eddy energy wax and wane in phase with the strength of the NECC. A map of the eddy energy for August–October, when the NECC is swift and quasi-steady, is very similar to that of the annual average. Thus, the distribution of maximum eddy energy in the mean is determined primarily by its distribution when the NECC is swiftest. The map for February–April is very different (Fig. 11b). The highest values, which are between 800 and 1200 cm^2 s^{-2}, form a thin band along the coast of South America from ~5°S to 13°N. In the mid-Atlantic, the region containing values >400 cm^2 s^{-2} has shrunk and lies roughly between 5°S and 5°N. No cluster of values over 800 cm^2 s^{-2} is found there.

An inspection of the monthly variation of velocity and eddy kinetic energy for a site between the NECC and SEC near 2–3°N, 25–30°W, shows that the eddy

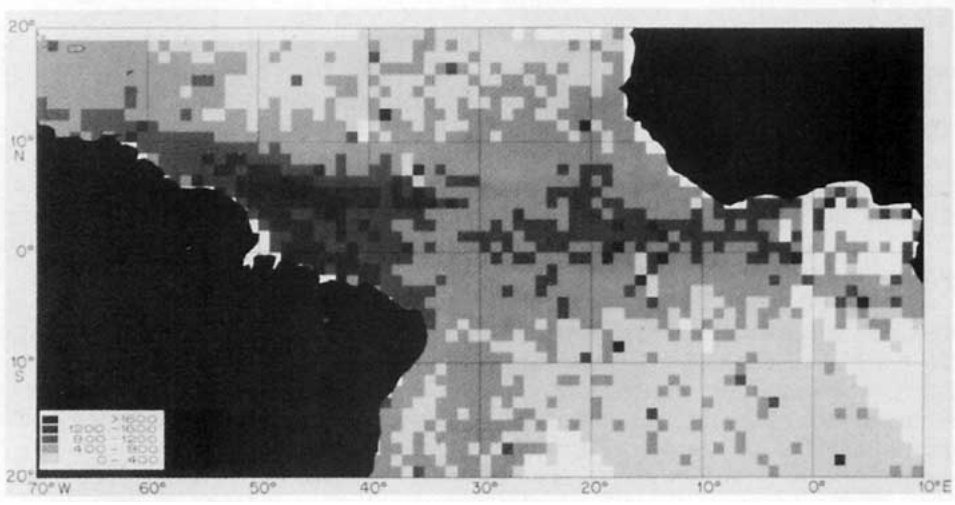

FIG. 11a. Distribution of eddy kinetic energy based on all the observations in each one-degree square. Squares that contained fewer than ten observations are left white. Highest values of eddy energy are observed in the western NECC near 5°N, 45°W where values are approximately 1800 cm^2 s^{-2}. A second area of high values (1000 cm^2 s^{-2}) is located between 0–4°N and 0–30°W, the region where strong shear between the NECC and the SEC occurs.

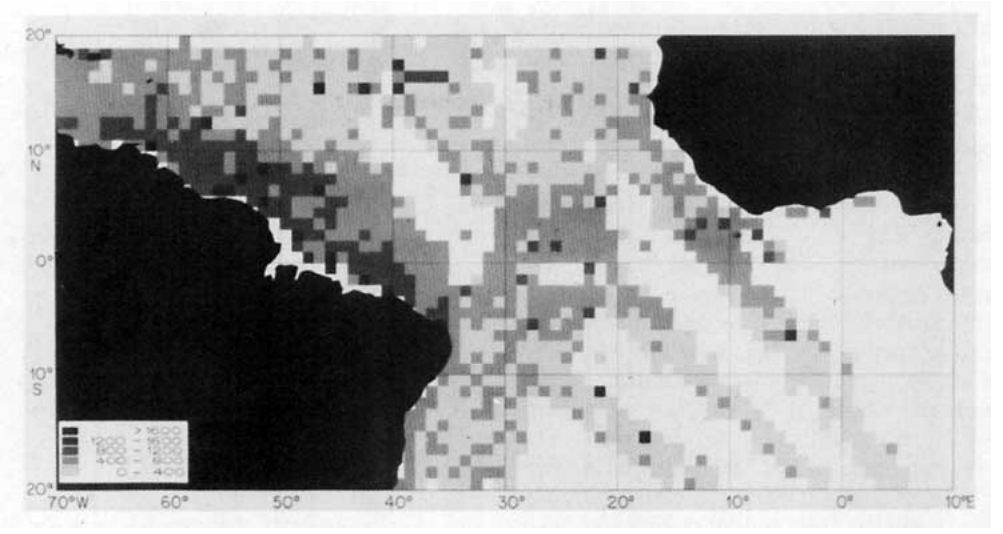

FIG. 11b. Distribution of eddy kinetic energy based on the observations from February–April when the NECC has disappeared. Greatly reduced energy levels are observed. (The map for August–October is similar to the annual average.)

energy is at a minimum of around 500 cm^2 s^{-2} in February–April, when the shear between the NECC and SEC is minimum. Eddy energy is maximum, ~1100 cm^2 s^{-2}, in June and July when the largest shear occurs. Approximately half of the eddy energy comes from the northward velocity variance, indicating that the peak is not just an artifact of grouping ship-drift measurements in the shear zone. (Some energy could also come from interannual fluctuations.)

The two regions of high eddy energy coincide with regions of strong shear in the zonal currents. Both are sites where current instability probably occurs, resulting in energetic mesoscale fluctuations (Philander, 1978). The most energetic fluctuation during GATE, a westward-propagating undulation with a period of about a month and wavelength of 1000 km, was observed in one of these regions, near 3°N, 23°W (Bubnov *et al.*, 1979). Strong mesoscale eddies have been observed in the other region (Cochrane *et al.*, 1979; Bruce *et al.*, 1983).

4. Discussion

Garzoli and Katz (1983) recently analyzed historical temperature data and plotted a time–longitude diagram of the seasonal variation of the meridional slope of the thermocline across the NECC. If geostrophy is assumed to be valid for the NECC, then the near-surface zonal velocity is proportional to the thermocline slope (ignoring Ekman flow). The variation of currents inferred from the thermocline slope and that measured by ship drift (Fig. 8a) are remarkably similar. They agree in showing the annual reversal in zonal currents; both show westward velocity between 25 and 45°W in February–June, with maxima near 40°W in April and May. Both show eastward velocity from July to January from 10 to 50°W. The main difference is that ship drifts show maximum eastward velocities of 30 cm s^{-1} in a zonal band across the Atlantic from July to September; the peak eastward velocity estimated from the geostrophic relation is centered at 40–45°W in October and November. The reversal observed by ship drift thus occurs about a month before that observed by temperature data.

Further confirmation of the general features of the reversal of currents is given by some freely drifting buoys (J. D. Cochrane, personal communication, 1983; Molinari, 1983; Garzoli and Katz, 1983) and the FGGE temperature data (Garzoli and Richardson, 1983). Considering the very different kinds and times of measurements, and techniques of data processing and averaging, the correspondence of results is astonishing. The implication is that in regions of large-scale and swift currents, the ship-drift technique is a good one for determining mean currents and their seasonal variations.

The relationship between the seasonally varying thermocline depth near the NECC and wind stress forcing have been explored by Garzoli and Katz (1983), Merle (1983) and Busalacchi and Picaut (1983). The major seasonal change in thermocline depth is a north–south tilting about a line that lies along the NECC and the mean position of the Intertropical Convergence Zone. This line separates two regions of large-amplitude thermocline variations which are approximately 180° out of phase. The main forcing is the curl of the wind stress, which is also 180° out of phase north and south of this line.

Vertical displacements of the thermocline are forced through the combined mechanisms of local Ekman pumping and the divergence of geostrophic currents (see Garzoli and Katz, 1983). Remote forcing in the east can cause thermocline displacements by means of westward propagating baroclinic Rossby waves.

Busalacchi and Picaut (1983) describe results of a numerical model that has a single baroclinic mode and a realistic coastline. The authors analyze the linear, dynamic response of the ocean to seasonal forcing by the measured wind flow over the tropical Atlantic. A curve they give of the monthly variation in NECC velocity agrees closely in maximum velocity and phase with the ship-drift data in the same area, but their NECC does not reverse direction. The implication is that more modes are required and/or nonlinearities are important. Cane (1979) and Philander and Pacanowski (1981) show that nonlinear effects and a southerly wind can result in an eastward jet downstream of the equator. Thus, part of the Atlantic NECC might be driven by southerly winds.

Acknowledgments. Funding for this work was provided by National Science Foundation Grant OCE-8208744. D. Carson drafted the figures and M. A. Lucas typed the manuscript. E. Katz, S. Schwartz, J. Toole, R. Weisberg, G. Reverdin and two anonymous reviewers made helpful suggestions on an earlier version. This paper was written while the first author was a visiting scientist at the Centre Océanologique de Bretagne in Brest. Alain Colin de Verdière arranged for the visit and the Centre National pour l'Exploitation des Océans provided funds.

REFERENCES

Anon, 1983: SEQUAL: A study of the equatorial Atlantic Ocean. *EOS Trans. Amer. Geophys. Union,* **63,** 218.

Beaglehole, J. C., Ed., 1955–67: *The Journals of Captain James Cook on His Voyages of Discovery.* Cambridge University Press, 4 Vols.

Boisvert, W. E., 1967: Major currents in the North and South Atlantic Oceans between 64°N and 60°S. Tech. Rep. TR-193, Naval Oceanographic Office, 105 pp. [NTIS AD-827-58619].

Bruce, J., J. Kerling and W. Beatty, 1983: On the North Brazilian eddy field. *Progress in Oceanography,* (in press).

Bubnov, V. A., and V. D. Egorikhin, 1979: Study of water circulation in the tropical Atlantic. *Deep-Sea Res., GATE Suppl. II,* **26,** 125–136.

——, V. M. Vasilenko and L. M. Krivelevich, 1979: The study of low-frequency variability of currents in the tropical Atlantic. *Deep-Sea Res., GATE Suppl. II,* 199–216.

Busalacchi, A. J., and J. Picaut, 1983: Seasonal variability from a model of the tropical Atlantic Ocean. *J. Phys. Oceanogr.,* **13,** 1564–1588.

Cane, M. A., 1979: The response of the western Equatorial Atlantic Ocean to simple wind stress patterns: I. Numerical results. *J. Mar. Res.,* **37,** 253–299.

Cochrane, J. D., F. J. Kelly, Jr. and C. R. Olling, 1979: Subthermocline countercurrents in the western equatorial Atlantic Ocean. *J. Phys. Oceanogr.,* **9,** 724–738.

Garzoli, S. L., and E. J. Katz, 1983: The forced annual reversal of the Atlantic North Equatorial Countercurrent. *J. Phys. Oceanogr.,* **13,** 2082–2090.

——, and P. L. Richardson, 1983: Seasonal variations of the Atlantic North Equatorial Countercurrent. *Trop. Ocean–Atmos. Newslett.,* **20,** 10–11.

Halpern, D., 1980: Variability of near-surface currents in the Atlantic North Equatorial Countercurrent during GATE. *J. Phys. Oceanogr.,* **10,** 1213–1220.

Hastenrath, S., and P. Lamb, 1977: *Climatic Atlas of the Tropical Atlantic and Eastern Pacific Ocean.* University of Wisconsin Press, 105 pp.

Katz, E. J., and S. Garzoli, 1982: Response of the western Equatorial Atlantic Ocean to an annual wind cycle. *J. Mar. Res.,* **40,** 307–327.

——, R. L. Molinari, D. E. Cartwright, P. Hisard, H. U. Lass and A. deMesquita, 1981: The seasonal transport of the equatorial undercurrent in the western Atlantic (during the Global Weather Experiment). *Oceanol. Acta,* **4,** 445–450.

Merle, J., 1983: Seasonal variability of subsurface thermal structure in the tropical Atlantic Ocean. *Hydrodynamics of the Equatorial Ocean,* J. C. J. Nihoul, Ed., Elsevier, 31–49.

Metcalf, W. G., and M. C. Stalcup, 1967: Origin of the Atlantic Equatorial Undercurrent. *J. Geophys. Res.,* **72,** 4959–4975.

Molinari, R. L., 1983: Satellite-tracked drifting buoy observations of near-surface currents and temperature in the central and western tropical Atlantic Ocean. *J. Geophys. Res.,* **88,** 4433–4438.

Neumann, G., 1960. Evidence for an equatorial undercurrent in the Atlantic Ocean. *Deep-Sea Res.,* **6,** 328–334.

Philander, S. G. H., 1978: Instabilities of zonal equatorial currents: II. *J. Geophys. Res.,* **83,** 3679–3682.

——, and R. C. Pacanowski, 1981: The oceanic response to cross-equatorial winds (with application to coastal upwelling in low latitudes). *Tellus,* **33,** 201–210.

Picaut, J., 1983: Propagation of the seasonal upwelling in the eastern equatorial Atlantic. *J. Phys. Oceanogr.,* **13,** 18–37.

Schumacher, A., 1940: Monatskarten des oberflachenstromung in Nordatlantischen Ozean. *Ann. Hydrogr. Mar. Meteor.,* **68,** 109–123.

Stalcup, M. C., and C. E. Parker, 1965: Drogue measurements of shallow currents on the equator in the western Atlantic Ocean. *Deep-Sea Res.,* **12,** 535–536.

Voigt, K., 1961: Äquatoriale Unterströmung auch Atlantik (Ergebnisse von Strömungsmessungen auf einer atlantischen Ankerstation der "Michail Lomonossov" am Äquator im Mai 1959). *Beitr. Meeresk,* **1,** 56–60.

Weisberg, R. H., and T. Y. Tang, 1983: Equatorial ocean response to growing and moving wind systems with application to the Atlantic. *J. Mar. Res.,* **41,** 461–486.

Wyrtki, K., L. Magaard and J. Hager, 1976: Eddy energy in the ocean. *J. Geophys. Res.,* **81,** 2641–2646.

——, E. Firing, D. Halpern, R. Knox, G. J. McNally, W. C. Patzert, E. D. Stroup, B. A. Taft and R. Williams, 1981: The Hawaii to Tahiti Shuttle Experiment. *Science,* **211,** 22–28.